



# Propagation Properties of a Tunable Impedance Waveguide

Olli Luukkonen, Constantin R. Simovski, Antti V. Räisänen,  
and Sergei A. Tretyakov

March 17, 2019

## Abstract

In this paper propagation properties of a parallel-plate waveguide with tunable artificial impedance surfaces as sidewalls are studied both analytically and numerically. The impedance surfaces comprise an array of patches over a dielectric slab with embedded metallic vias. The tunability of surfaces is achieved with varactors. Simple design equations for tunable artificial impedance surfaces are presented. The analytical results are verified with numerical simulations. The results of this paper show that although phase shifting is achieved by using tunable impedance surfaces as sidewalls of waveguides, unwanted mode conversion occurs as well.

## 1 Introduction

Artificial impedance surfaces [1–9] have received a lot of interest since the beginning of the last decade. The artificial impedance surfaces are composed in general of a capacitive grid on top of a thin metal-backed dielectric substrate.

---

\*O. Luukkonen, C. R. Simovski, A. V. Räisänen, and S. A. Tretyakov are with are with Radio Laboratory/SMARAD, TKK Helsinki University of Technology, P.O. 3000, FI-02015 TKK, Finland (email: olli.luukkonen@tkk.fi)

†C. Simovski is also with Department of Physics, St. Petersburg Institute of Fine Mechanics and Optics, 197101, Sablinskaya 14, St. Petersburg, Russia.

The substrate may include vias, as in [2, 4], or not [9–11]. Nevertheless, the purpose in both types of designs is to use the metal-backed substrate to provide an inductive response that together with the capacitive grid would create a resonant structure. Because of the resonant nature such impedance surfaces are commonly referred to as high impedance surfaces.

Close to the resonance frequency the (input) surface impedance of an artificial impedance surface is high and the surface behaves as a magnetic conductor. This feature has been utilized in waveguide structures to create quasi-TEM waveguides [11, 12]. In [11] the authors designed an artificial impedance surface, utilized the surface as a sidewall of a rectangular waveguide, and both numerically and experimentally showed a uniform field distribution in the vicinity of the resonance frequency of the surface. The uniform power density was experimentally demonstrated in [12] as well. In both [11] and [12] the impedance surface designs were non-tunable and the properties of the surfaces were modeled with lumped element models. In addition to the lumped element models, also layered homogeneous material model has been developed [13, 14] to predict the behavior of a non-tunable high-impedance surfaces.

Recently some research has been devoted to electrical tunability of high-impedance surfaces [15–19]. In [15] tunability of the high-impedance surface was realized by connecting adjacent patches to each other by voltage controllable varactors. The purpose in [15] was to create reflection-phase gradients on the surface in order to use the surface as a reflector antenna capable for beam steering. The beam steering was verified experimentally in that paper. The same tunable high-impedance surface design has been used in other applications as well such as tunable leaky-wave antennas [16]. In [17] adjacent capacitive strips were connected to each other with varactor diodes. The resulting electrically tunable high-impedance surface was used as a sidewall of a rectangular waveguide that was used for phase shifting purposes. A 360°-degree phase shift was achieved experimentally by changing the value of the bias voltage between 0 V and 9.0 V. In addition to the varactor-based tunable phase shifters also a MEMS-based tunable high-impedance surface phase shifter has been proposed in [19].

In [15–18] the analysis of the tunable high-impedance surface has been done by using a simplistic lumped-element model of the surface, similar to that of [20]. The lumped-element model [20] offers guidelines for the design of a tunable high-impedance surface, but cannot be used for an accurate analysis of the surface. This applies also to applications based on the use of

high-impedance surfaces. In [21] a similar tunable high-impedance surface structure as in [15] was studied. In [21] an equivalent circuit model is used to approximate the effect of the varactor resistance to the reflection characteristic of the high-impedance surface. Although bringing insight to the effect of losses of the varactor-based tunable high-impedance surface, the model in [21] is restricted only to the normal incidence.

Although the subject of tunable high-impedance surfaces and impedance waveguides based on them has been addressed in the literature, no analytical models accurately describing the characteristics of tunable high-impedance surfaces have been presented in the open literature to the authors knowledge. Yet an accurate model would serve as a useful design tool for the tunable high-impedance surface applications, such as the tunable impedance waveguide. This serves as one of the motivations for this paper. In addition, as there is interest towards tunable impedance waveguides, the authors of this paper feel that knowledge of the propagation properties of a tunable high-impedance surface waveguide is needed.

Analysis of dispersion of a rectangular waveguide with impedance sidewalls comprising non-tunable dipole-like frequency selective surfaces (FSS) on a metal backed dielectric slab have been studied also in [22]. In [22] the analysis is carried out numerically by the method of moments. The authors provide dispersion diagrams, but one of the key points of this paper, that is, the conversion of the propagation properties from one of the metallic waveguide modes to another in the vicinity of the resonance frequency of the high-impedance surface, is not evident from these diagrams.

In this paper we study the propagation properties of a tunable (impedance) waveguide. The waveguide has tunable artificial impedance surfaces as sidewalls. The high-impedance surface used here is similar to those in [15, 16]: The surface comprises metal patches over a dielectric slab with embedded vias and the patches are connected to each other by tunable varactors. We first write down the simple analytical expressions for the varactor-tunable high-impedance surface. Using this analytical model we will study the propagation properties of an impedance waveguide having either one or two tunable impedance surface sidewalls. The numerical simulations verify the analytical results and show that the analytical model describes accurately the properties of tunable impedance surfaces. In particular, we will show that “mode conversion” occurs in the waveguide when the resonance frequency of the tunable impedance surfaces is tuned gradually over the operational frequency of the system.

## 2 A waveguide with arbitrary impedance boundaries

We consider the propagation behavior of a parallel-plate waveguide having tunable impedance surfaces as sidewalls and study it using the plane-wave interpretation. The two-dimensional waveguide is illustrated in Fig. 1. The number of the varying transversal wave numbers is limited to one as no propagation happens in the  $x$ -direction. The waveguide is confined in the  $y$ -direction by sidewalls that can be modeled with an impedance surface  $Z_{\text{inp}}^+$  or  $Z_{\text{inp}}^-$  that depend on the propagation factor  $\beta$ . The notation  $\pm$  refers to the upper/lower surface, respectively, and the subscript “inp” refers to the (input) surface impedance of the high-impedance surface.

The longitudinal components of the TM and TE modes can be written in our two-dimensional waveguide as

$$E_z = (Ae^{-jk_y y} + Be^{jk_y y}), \quad (1)$$

$$H_z = (Ce^{-jk_y y} - De^{jk_y y}), \quad (2)$$

respectively. In (1) and (2)  $k_y = \sqrt{k^2 - \beta^2}$  is the transverse wave number,  $k$  is the wave number, and  $\beta$  is the propagation constant along the waveguide. Furthermore,  $A$ ,  $B$ ,  $C$ , and  $D$  are the amplitudes of the waves (propagating along two directions). The transverse components can be expressed through the gradients of the longitudinal field components using (e.g. [23])

$$\mathbf{H}_t = \frac{1}{\beta^2 - k^2} (j\beta \nabla_t H_z + j\omega \varepsilon \mathbf{z}_0 \times \nabla_t E_z), \quad (3)$$

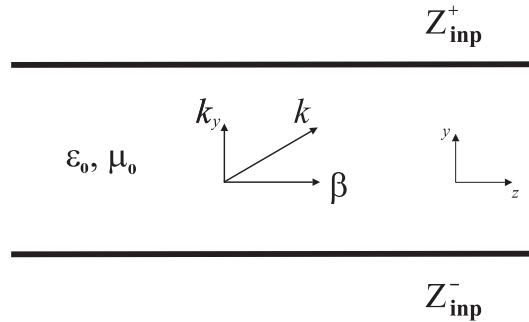


Figure 1: Illustration of the two dimensional waveguide confined by two impedance surfaces.

$$\mathbf{E}_t = \frac{1}{\beta^2 - k^2} (j\beta \nabla_t E_z + j\omega \varepsilon \mathbf{z}_0 \times \nabla_t H_z), \quad (4)$$

where  $\nabla_t$  is the nabla operator acting only on the transverse (with respect to the propagation direction) coordinates,  $\varepsilon$  is the dielectric constant of the medium in the waveguide, and  $\mathbf{z}_0$  is the unit vector directed along the waveguide axis.

The boundary conditions for the waveguide sidewalls at  $y = 0$  and  $y = d$  (Fig. 1) can be written, respectively, as

$$\mathbf{E}_t = \mathbf{n} \times \mathbf{H} Z_{\text{inp}}^-, \quad (5)$$

$$\mathbf{E}_t = -\mathbf{n} \times \mathbf{H} Z_{\text{inp}}^+, \quad (6)$$

where  $\mathbf{n}$  is the normal vector of the waveguide sidewalls and  $\mathbf{E}_t$  are the electric field components tangential to the surface. In this particular case  $\mathbf{n}$  is the unit vector along the  $y$ -axis.

By solving the transversal field components using (1), (2), (3) and (4), writing down the boundary conditions on both boundaries, and solving the resulting  $2 \times 2$  matrix for non-trivial solutions, we get a dispersion equation that needs to be solved numerically. The dispersion equations for TM- and TE-modes read, respectively:

$$\frac{\left(1 - \frac{\omega \varepsilon k_y}{\beta^2 - k^2} Z_{\text{inp}}^+\right) \left(1 - \frac{\omega \varepsilon k_y}{\beta^2 - k^2} Z_{\text{inp}}^-\right)}{\left(1 + \frac{\omega \varepsilon k_y}{\beta^2 - k^2} Z_{\text{inp}}^+\right) \left(1 + \frac{\omega \varepsilon k_y}{\beta^2 - k^2} Z_{\text{inp}}^-\right)} = e^{-j2k_y d}, \quad (7)$$

$$\frac{\left(\frac{\omega \mu k_y}{\beta^2 - k^2} - Z_{\text{inp}}^-\right) \left(\frac{\omega \mu k_y}{\beta^2 - k^2} - Z_{\text{inp}}^+\right)}{\left(\frac{\omega \mu k_y}{\beta^2 - k^2} + Z_{\text{inp}}^-\right) \left(\frac{\omega \mu k_y}{\beta^2 - k^2} + Z_{\text{inp}}^+\right)} = e^{-j2k_y d}. \quad (8)$$

To simplify the dispersion equations, we write  $\frac{\omega \varepsilon k_y}{\beta^2 - k^2} = -\frac{1}{\eta} \frac{k}{k_y}$  and  $\frac{\omega \mu k_y}{\beta^2 - k^2} = -\eta \frac{k}{k_y}$ , where  $\eta$  is the plane wave impedance of the medium in the waveguide. After some mathematical manipulation the dispersion equation for TE modes reduces to

$$\tan(k_y d) = j\eta \frac{k}{k_y} \frac{Z_{\text{inp}}^+ + Z_{\text{inp}}^-}{\eta^2 \frac{k^2}{k_y^2} + Z_{\text{inp}}^+ Z_{\text{inp}}^-}. \quad (9)$$

For TM modes the dispersion equation reads

$$\tan(k_y d) = j\eta \frac{k_y}{k} \frac{Z_{\text{inp}}^+ + Z_{\text{inp}}^-}{\eta^2 \frac{k_y^2}{k^2} + Z_{\text{inp}}^+ Z_{\text{inp}}^-}. \quad (10)$$

Clearly, by replacing  $Z_{\text{inp}}^{\pm} = 0$  in (9) and (10) we get  $k_y = n \cdot \pi$ , for  $n = 0, 1, 2, \dots$ , which are the results for a metallic parallel-plate waveguide.

### 3 Tunable artificial impedance surfaces

The dispersion equations (9) and (10) have been derived for arbitrary surface impedances. In this paper a mushroom type of artificial impedance surface (see Fig. 2), proposed in [2], is studied as a possible particular realization. The sidewalls of the waveguide are covered with artificial impedance surfaces that are comprised of metallic rectangular patches and metal-backed dielectric substrates with embedded vias. The input (surface) impedance of an artificial impedance surface can be modeled through a transmission-line model shown in Fig. 3. The input impedance is hence a parallel connection of the grid impedance of an array of patches and the surface impedance of a metal-backed dielectric slab with embedded vias:

$$Z_{\text{inp}}^{-1} = Z_g^{-1} + Z_s^{-1}. \quad (11)$$

In the above equation subscript g refers to the grid impedance of an array of patches and s refers to the surface impedance of the substrate.

A simple and accurate analytical model for the mushroom-type impedance surface is available [7]. In [7] the mushroom structures comprised arrays of patches on top of a dielectric layer. However, in this paper we consider mushroom structures that comprise arrays of patches on top of a metal-backed dielectric slab with embedded metallic vias. The vias are needed to provide the bias voltage for the varactors that are used to vary the capacitance between the adjacent strips or patches (as in [15,17]). For TE modes the electric field component is perpendicular to the vias and, in the case of thin vias, does not excite them. It can be concluded that the analytical model [7] can be readily applied for TE modes in the case of embedded vias as well. However, for TM modes the electric field has a parallel component to the vias. In this case it is possible to replace the metallic vias in dielectric slab with an effective wire medium model [3,5].

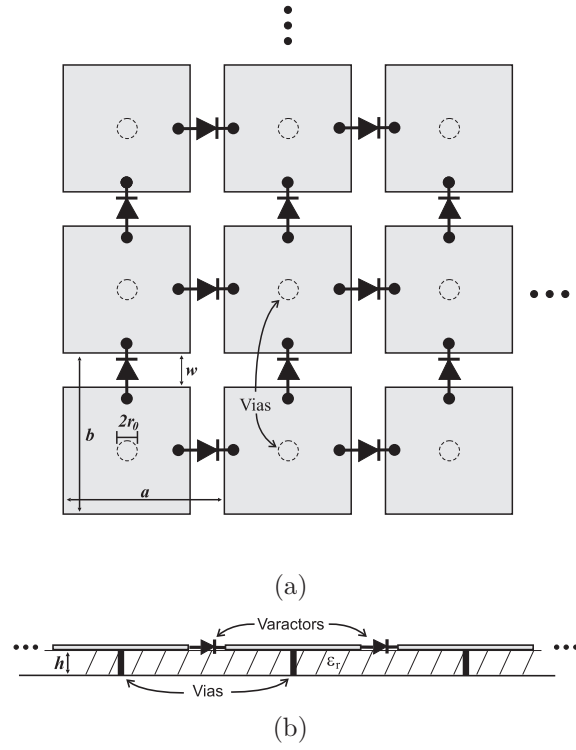


Figure 2: (a) A view from the top of the Sievenpiper mushroom structure loaded with varactors. (b) A view from the side.

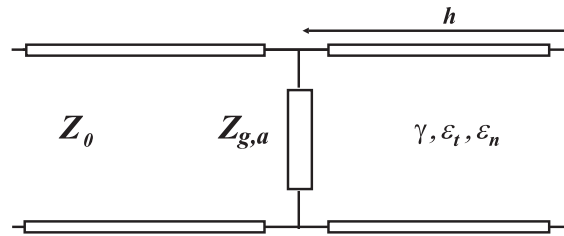


Figure 3: A transmission-line model for modeling artificial impedance surfaces.

### 3.1 Surface impedance of the dielectric slab with embedded vias

The surface impedance for a wire medium comprising thin perfectly conducting wires reads [5]:

$$Z_s^{\text{TM}} = j\omega\mu_0 \frac{\tan(\gamma_{\text{TM}}h)}{\gamma_{\text{TM}}} \frac{k^2 - \beta^2 - k_p^2}{k^2 - k_p^2}, \quad (12)$$

where  $k = k_0\sqrt{\varepsilon_r}$  is the wave number in the host medium,  $\varepsilon_t$  is the relative permittivity for the fields along the transverse plane,

$$\gamma_{\text{TM}} = \omega^2\varepsilon_0\varepsilon_t\mu_0 - \frac{\varepsilon_t}{\varepsilon_n}\beta^2, \quad (13)$$

and

$$k_p = a\sqrt{\frac{1}{2\pi} \ln \frac{a^2}{4r_0(a-r_0)}}. \quad (14)$$

Furthermore,  $a$  is the period of the wires,  $r_0$  is the radius of the wires, and the relative permittivity for the fields along the normal of the medium

$$\varepsilon_n = \varepsilon_t \left( 1 - \frac{k_p^2}{k^2\varepsilon_t} \right). \quad (15)$$

In the case when the vias are thin and vertically oriented the relative permittivity for the fields along the transversal plane,  $\varepsilon_t$ , equals to the relative permittivity of the host medium,  $\varepsilon_r$ .

For TE modes the electric field is perpendicular to the thin metallic wires. In this case the electric field does not excite the wires as discussed above and the surface impedance for the TE mode is that of a metal-backed dielectric slab ([5]):

$$Z_s^{\text{TE}} = j\omega\mu_0 \frac{\tan(k_y\sqrt{\varepsilon_r}h)}{k_y\sqrt{\varepsilon_r}}. \quad (16)$$

### 3.2 The grid impedance

The grid impedance for an array of patches can be calculated through the approximative Babinet principle using the averaged boundary conditions for a mesh of wires or strips. The averaged boundary condition for a mesh of

strips is available (e.g., in [5]). The grid impedance for an array of ideally conducting patches on top of a dielectric substrate reads [7]:

$$Z_g^{\text{TM}} = -j \frac{\eta_{\text{eff}}}{2\alpha}, \quad (17)$$

$$Z_g^{\text{TE}} = -j \frac{\eta_{\text{eff}}}{2\alpha \left(1 - \frac{k_0^2 \sin^2 \theta b}{k_{\text{eff}}^2 \left(1 + \frac{b}{a}\right)}\right)}, \quad (18)$$

where the effective wave impedance  $\eta_{\text{eff}} = \frac{\eta_0}{\sqrt{\epsilon_{\text{eff}}}}$ , the effective wave number  $k_{\text{eff}} = k_0 \sqrt{\epsilon_{\text{eff}}}$ ,  $\sin^2(\theta) = \frac{k_0^2 - k_y^2}{k_0^2}$ , and  $b$  and  $a$  are the dimensions of the unit cell of the structure along  $x$ - and  $y$ -axis, respectively. For simplicity, only cases for which  $a = b$  are considered in this paper. Further,  $\alpha$  is the *grid parameter*:

$$\alpha = \frac{k_{\text{eff}} b}{\pi} \ln \left( \frac{1}{\sin \left( \frac{\pi w}{2b} \right)} \right), \quad (19)$$

where  $w$  is the gap between the adjacent patches (Fig. 2). The effective relative permittivity for the array of patches or grid of strips on the boundary between the media having relative permittivities of  $\epsilon_1$  and  $\epsilon_2$  reads [25]:

$$\epsilon_{\text{eff}} = \frac{\epsilon_1 + \epsilon_2}{2}. \quad (20)$$

In this paper the array of patches is located on a boundary between free space and wire medium. From above it is known that in a wire medium the fields along the transversal and normal axis have different effective relative permittivities. For an array of patches the electric fields are concentrated mainly between the adjacent patches, transverse with respect to the vias, and the effect of the vias to the electric response is weak. For this reason the transversal relative permittivity of the wire medium is used in (20).

The grid impedances (17) and (18) can be written in a lumped-element form as:

$$Z_g^{\text{TM,TE}} = \frac{1}{j\omega C_g^{\text{TM,TE}}}, \quad (21)$$

where  $C_g^{\text{TM,TE}}$  is the grid capacitance for the TM- or TE-polarized incidence fields. Using (17), (18), and (21) the grid capacitance for an array of patches can be written as:

$$C_g^{\text{TM}} = \frac{b\epsilon_0 (\epsilon_1 + \epsilon_2)}{\pi} \ln \left( \frac{1}{\sin \left( \frac{\pi w}{2b} \right)} \right), \quad (22)$$

$$C_g^{\text{TE}} = \frac{b\varepsilon_0(\varepsilon_1 + \varepsilon_2)}{\pi} \ln \left( \frac{1}{\sin \left( \frac{\pi w}{2b} \right)} \right) \left( 1 - \frac{k_0^2 \sin^2 \theta}{k_{\text{eff}}^2} \right). \quad (23)$$

In (23) the condition  $a = b$  has been taken into consideration.

### 3.3 Tunable capacitance

The above formulas for the capacitive grid impedances hold for ideally conducting patches. Although the capacitive impedance is derived through averaged fields on the grid, we may consider a lumped-element model here. This way the capacitance of the varactors, that are used for tuning, can be included in the analysis easily: The additional capacitance of the varactors is connected parallel with the grid capacitance and the total impedance of a unit cell is thus a parallel connection of these impedances. Hence the total grid capacitance of the array of patches with varactors can be written as:

$$C_{\text{tot}} = C_g + C_{\text{var}}, \quad (24)$$

where  $C_g$  is the grid capacitance for an array of ideally conducting patches and  $C_{\text{var}}$  is the capacitance of the tunable varactor. The total grid impedance thus reads:

$$Z_g = \frac{1}{j\omega C_{\text{tot}}} = \frac{1}{j\omega (C_g + C_{\text{var}})}. \quad (25)$$

In order to most effectively tune the grid impedance, the capacitance of the varactor needs obviously to be considerably larger than the grid capacitance.

The effect of the varactor resistance to the performance of a tunable high-impedance surface has been studied in [21]. It is possible to include the effect of the diode resistance to the above analysis in a similar way as done in [21]. However, this is considered to be out of the scope of this paper.

## 4 Tunable parallel-plate waveguide

In this section the propagation properties of a parallel-plate waveguide having either one or two artificial impedance surfaces are studied analytically. The analytical results are verified with simulations using Ansoft's High Frequency Structure Simulator (HFSS).

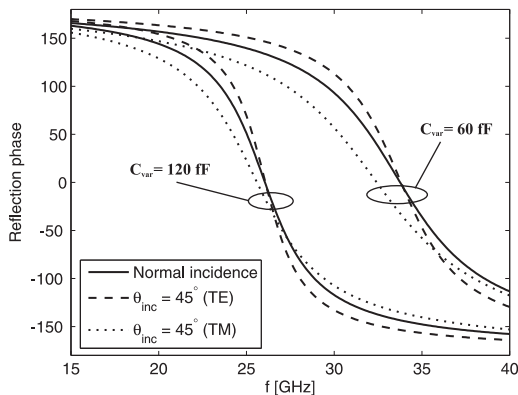
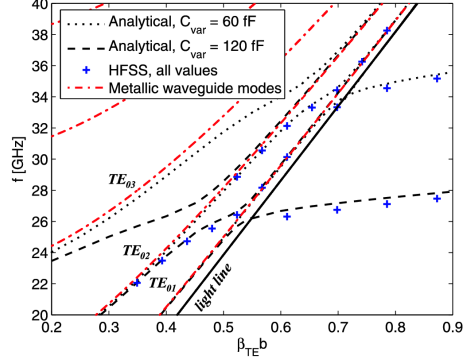


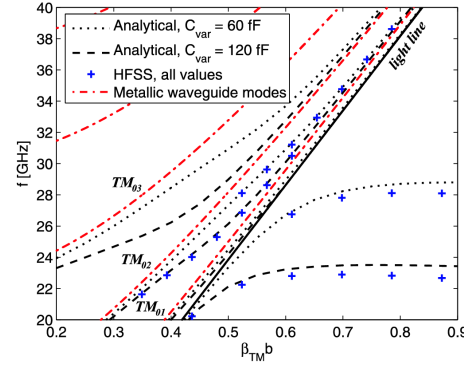
Figure 4: The reflection phases for normal incidence for different values of varactor capacitance.

The impedance surfaces for the waveguides are designed for the lower millimeter wave region, namely Ka-band (26–40 GHz). Following the notations in Fig. 2, the parameters of the studied artificial impedance surface are:  $a = b = 1$  mm,  $w = 0.1$  mm,  $h = 0.2$  mm, and  $\epsilon_r = \epsilon_2 = 4$ . The medium inside the impedance waveguide is air ( $\epsilon = \epsilon_1 = 1$ ). The varactors on each edge of the patch were modeled with lumped capacitive sheets whose value of capacitance was changed case sensitively. The impedance surface was placed inside a unit cell of a parallel plate waveguide. The periodicity in the simulation model was achieved by using the periodical boundary conditions available in HFSS.

According to (22) the grid capacitance of the designed impedance surface is approximately 26 fF. Based on this information and on the frequency band of interest the capacitance of the varactors is varied from 60 fF to 120 fF; with these values the resonance frequency of the surface for the normal incidence appears to be approximately at 34 GHz and 26 GHz, respectively. Furthermore, the capacitance of the varactors is considerably larger than the grid capacitance, as discussed earlier. The reflection phases of the surface for different values of  $C_{\text{var}}$  are shown in Fig. 4 for the normal incidence and for oblique incidence at  $45^\circ$ . Clearly the bandwidth for the TE polarization becomes smaller and the bandwidth for the TM polarization larger as the angle of incidence grows. The effect of this to the propagation properties of the impedance waveguide will be discussed later.



(a)



(b)

Figure 5: Color online. (a) The propagation properties of an impedance waveguide with one tunable impedance surface for TE modes. (b) The propagation properties of an impedance waveguide with one tunable impedance surface for TM modes. The fundamental modes of metal waveguide are plotted with dash-dot lines.  $\beta_{TE}$  and  $\beta_{TM}$  refer here to the propagation constants of the TE and TM modes, respectively.

Before moving on to the interpretation of the results, the terms used in the following paragraphs need to be clarified. It is natural to use the modes propagating in a metallic waveguide as reference cases when studying the propagation properties of an impedance waveguide. Therefore the modes propagating in a metallic waveguide will be referred as *fundamental modes* from here on in order to distinguish them from the modes of an impedance

waveguide (referred plainly as *modes*).

The dispersion curves of a 20-mm high parallel-plate waveguide with one tunable impedance surface are shown in Fig. 5. The second surface is perfectly conducting metal. The fundamental modes of a parallel-plate waveguide are shown with dash-dot lines. The simulation results have been marked with crosses in Fig. 5. The concurrence between the analytical and numerical results is very good. The height of the waveguide was chosen so that many fundamental modes would propagate in the waveguide in the frequency band of 26–40 GHz.

In Fig. 5 near the resonance frequency of the impedance surface a 180° “mode conversion” is observed for both polarizations. The propagating wave exhibits a 180° phase shift while the mode morphs from one fundamental mode to another. This is due to the change of the reflection phase of the impedance surface. For instance, a wave propagating at 27.5 GHz near the second fundamental mode, TE<sub>02</sub> in Fig. 5(a), morphs to the first fundamental mode, TE<sub>01</sub>, when the varactor capacitance is changed gradually from 60 fF to 120 fF. Similar behavior occurs for higher-order modes and for TM<sub>01</sub> as well. The field pattern of the TE<sub>01</sub> mode is plotted in Fig. 6.

The mode conversion is seen to happen more gradually for the TM modes in Fig. 5 (b) than for the TE modes in Fig. 5 (a). This is because the bandwidth of the high-impedance surface becomes wider for TM polarized fields than for TE polarized fields as the angle of incidence grows, as discussed above. This creates an advantage for the TE modes over the TM modes in tunable impedance waveguide applications: The needed range of tuning of the resonant frequency of the high-impedance surface is smaller for the TE modes than for the TM modes in impedance waveguide applications.

The dispersion curve for a parallel-plate waveguide having two tunable impedance surfaces is shown in Fig. 7. Similar mode conversion is seen as in the case of just one impedance surface. However, instead of a 180° mode conversion discussed earlier, a 360° mode conversion occurs. This is simply because both impedance surfaces induce a 180° mode conversion.

The larger mode conversion offers interesting properties in the vicinity of the resonance frequency of the surface: Both TE<sub>01</sub> and TE<sub>02</sub> modes cross the light line at only slightly different points. The TE<sub>01</sub> mode crosses the light line at  $\beta b = 0.71$ ,  $f = 33.9$  GHz whereas the TE<sub>02</sub> mode crosses it at  $\beta b = 0.77$ ,  $f = 34.2$  GHz. The field patterns of the TE<sub>01</sub> and TE<sub>02</sub> modes are shown in Figs. 8 and 9, respectively, for the case when  $C_{\text{var}} = 60$  pF.

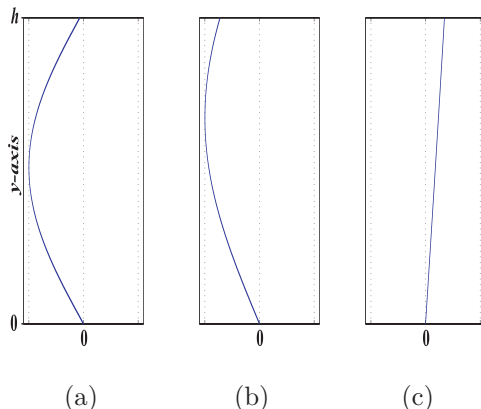


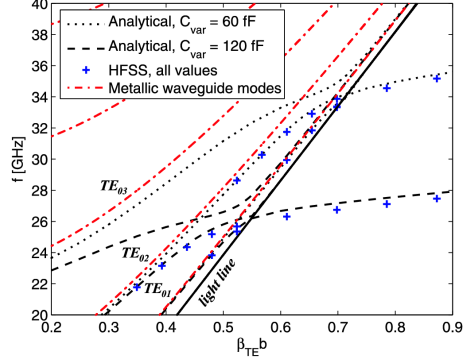
Figure 6: Color online. The magnitude of the electrical field component along x-axis for the  $TE_{01}$  mode at points (a)  $\beta b = 0.5$ ,  $f = 25.0$  GHz (b)  $\beta b = 0.69$ ,  $f = 33.5$  GHz, and (c)  $\beta b = 0.71$ ,  $f = 34.0$  GHz

## 5 Discussion and conclusions

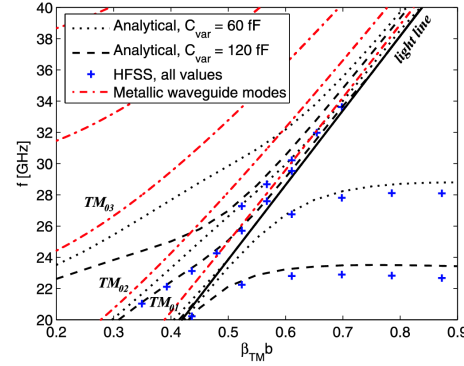
The propagation properties of impedance waveguide having either one or two tunable impedance surfaces have been studied. Design formulas for a particular type of tunable impedance surface have been presented. The design formulas are easily applicable for different types of tunable impedance surfaces as well. According to the results at the vicinity of the resonance frequency of the impedance surfaces mode conversion can occur.

As an example, let us consider a waveguide with tunable high-impedance surfaces as sidewalls that is used as a phase shifter. The phase shifter is ended from both sides with metallic waveguides that have exactly the same dimensions as the phase shifter. The dimensions of the waveguides are such that many modes can propagate in them. The phase shifter is fed with  $TE_{01}$  mode from the metallic waveguide. In order to minimize reflections from the transition interface between the feeding metallic waveguide and the phase shifter, and to make sure that most of power is coupled to the wanted mode, impedance of the tunable high-impedance surfaces is changed gradually from zero to higher values, similarly as in tapered waveguides. The impedance is varied by changing the resonance frequency of the surface.

When the resonance frequency of the high-impedance surface is lowered gradually through the operational frequency, the reflection phase of the sur-



(a)



(b)

Figure 7: Color online. (a) The propagation properties of an impedance waveguide with two tunable impedance surfaces for TE modes. (b) The propagation properties of an impedance waveguide with two tunable impedance surfaces for TM modes. The fundamental modes of metal waveguide are plotted with dash-dot lines.  $\beta_{\text{TE}}$  and  $\beta_{\text{TM}}$  refer here to the propagation constants of the TE and TM modes, respectively.

face changes from  $+180^\circ$  to  $-180^\circ$  (see Fig. 4) and vice versa, if the resonance frequency is raised. In the case of two impedance surfaces this would equal to the change of field patterns in the waveguide from  $\text{TE}_{03}$  to  $\text{TE}_{01}$  (or from  $\text{TE}_{01}$  to  $\text{TE}_{03}$ , if the resonance frequency is raised), see Fig. 7 (a).

While gradually raising the resonance frequency of the impedance surface through the operational frequency, the power will morph from the fed  $\text{TE}_{01}$

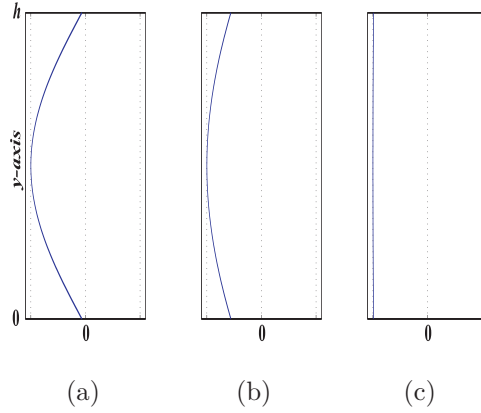


Figure 8: Color online. The magnitude of the electrical field component along x-axis for the  $TE_{01}$  mode at points (a)  $\beta b = 0.5$ ,  $f = 24.9$  GHz (b)  $\beta b = 0.69$ ,  $f = 33.3$  GHz, and (c)  $\beta b = 0.71$ ,  $f = 33.9$  GHz

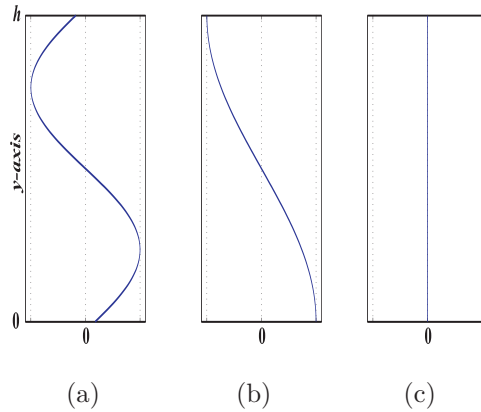


Figure 9: Color online. The magnitude of the electrical field component along x-axis for the  $TE_{02}$  mode at points (a)  $\beta b = 0.5$ ,  $f = 27.7$  GHz (b)  $\beta b = 0.69$ ,  $f = 33.9$  GHz, and (c)  $\beta b = 0.77$ ,  $f = 34.2$  GHz

mode to the  $TE_{03}$  mode in the phase shifter and a  $360^\circ$  phase shift will occur. On the interface of the second transition most of the power from the  $TE_{03}$  mode in the phase shifter would obviously couple to the  $TE_{03}$  mode in the metallic waveguide. As a result an additional  $360^\circ$  phase shift has been attained, but the mode has been converted from the original  $TE_{01}$  mode to the  $TE_{03}$  mode. For most phase shifting applications this is seldom a wanted

feature.

In order to keep most of the power in the original mode, the transition can be reversed, that is, the resonance frequency of the impedance surface is gradually lowered before the second transition interface is reached. In this case the additional  $360^\circ$  phase shift would be canceled and the attained phase shift would be determined from the length of the phase shifter and the difference between the propagation constants in the metallic waveguide and in the phase shifter.

Obviously by tuning the impedance of the sidewalls it is possible to change the propagation properties of a waveguide. This property can be used to create impedance waveguide phase shifters, as in [17]. While shifting the resonance frequency of the impedance surfaces on the sidewalls of waveguide through the operational frequency mode conversion occurs, as discussed above. In addition to the  $180^\circ$  or  $360^\circ$  phase shift, the mode is converted from one fundamental mode to another as well.

## References

- [1] P.-S. Kildal, "Artificially soft and hard surfaces in electromagnetics," *IEEE Transactions on Antennas and Propagation*, vol. 38, no. 10, pp. 1537–1544, Oct. 1990.
- [2] D. Sievenpiper, L. Zhang, R. F. J. Broas, N. G. Alexopolous, and E. Yablonovitch, "High-impedance electromagnetic surfaces with a forbidden frequency band," *IEEE Transactions on Microwave Theory and Techniques*, vol. 47, no. 11, pp. 2059–2074, Nov. 1999.
- [3] R. E. Diaz, J. T. Aberle, and W. E. McKinzie, "TM mode analysis of a Sievenpiper high-impedance reactive surface," *IEEE Antenna and Propagation International Symposium*, vol. 1, pp. 327–330, July 2000.
- [4] S. A. Tretyakov, and C. R. Simovski, "Dynamic model of artificial reactive impedance surfaces," *Journal of Electromagnetic Waves and Applications*, vol. 17, no. 1, pp. 131–145, Nov. 2003.
- [5] S. A. Tretyakov, *Analytical Modelling in Applied Electromagnetics*, London, UK, Artech House, 2003.

- [6] S. A. Tretyakov and S. I. Maslovski, “Thin absorbing structure for all incidence angles based on the use of a high-impedance surface,” *Microwave and Optical Technology Letters*, vol. 38, no. 3, pp. 175–178, Jan. 2003.
- [7] O. Luukkonen, C. Simovski, G. Granet, G. Goussetis, D. Lioubtchenko, A. V. Räisänen, and S. Tretyakov, “Simple and accurate analytical model of planar grids and high-impedance surfaces comprising metal strips or patches,” *submitted to IEEE Transactions on Antennas and Propagation*, preprint available at <http://arxiv.org/abs/0705.3548>.
- [8] C. R. Simovski, P. de Maagt, S. A. Tretyakov, M. Paquay, and A. A. Sochava, “Angular stabilisation of resonant frequency of artificial magnetic conductors for TE-incidence,” *Electronics Letters*, vol. 40, no. 2, pp. 92–93, Jan. 2004.
- [9] G. Goussetis, A. P. Feresidis, and J. C. Vardaxoglou, “Tailoring the AMC and EBG characteristics of periodic metallic arrays printed on grounded dielectric substrate,” *IEEE Transactions on Antennas and Propagation*, vol. 54, no. 1, pp. 82–89, Jan. 2006.
- [10] S. Maci, M. Caiazzo, A. Cucini, and M. Casaletti, “A pole-zero matching method for EBG surfaces composed of a dipole FSS printed on a grounded dielectric slab,” *IEEE Transactions on Antennas and Propagation*, vol. 53, no. 1, pp. 70–81, Jan. 2005.
- [11] F.-R. Yang, K.-P. Ma, Y. Qian, and T. Itoh, “A novel TEM waveguide using uniplanar compact photonic-bandgap (UC-PBG) structure,” *IEEE Transactions on Microwave Theory and Techniques*, vol. 47, no. 11, pp. 2092–2098, Nov. 1999.
- [12] J. A. Higgins, M. Kim, J. B. Hacker, and D. Sievenpiper, “The application of photonic crystals to quasi-optic amplifier,” *IEEE Transactions on Microwave Theory and Techniques*, vol. 47, no. 11, pp. 2139–2143, Nov. 1999.
- [13] S. Clavijo, R. E. Díaz, and W. E. McKinzie, III, “Design methodology for Sievenpiper high-impedance surfaces: An artificial magnetic conductor for positive gain electrically small antennas,” *IEEE Transactions on Antennas and Propagation*, vol. 51, no. 10, pp. 2678–2690, Oct. 2003.

- [14] J. M. Hao, L. Zhou, and C. T. Chan, “An effective medium model for high-impedance surfaces,” *Applied Physics A*, vol. 87, no. 2, pp. 281–284, Jan. 2007.
- [15] D. F. Sievenpiper, J. H. Schaffner, H. J. Song, R. Y. Loo, and G. Tantonan, “Two-dimensional beam steering using an electrically tunable impedance surface,” *IEEE Transactions on Antennas and Propagation*, vol. 51, no. 10, pp. 2713–2722, Oct. 2003.
- [16] D. F. Sievenpiper, “Forward and backward leaky wave radiation with large effective aperture from an electronically tunable surface,” *IEEE Transactions on Antennas and Propagation*, vol. 53, no. 1, pp. 236–247, Jan. 2005.
- [17] J. A. Higgins, H. Xin, A. Sailer, and M. Rosker, “Ka-band waveguide phase shifter using tunable electromagnetic crystal sidewalls,” *IEEE Transactions on Microwave Theory and Techniques*, vol. 51, no. 4, pp. 1281–1288, April 2003.
- [18] H. Xin, J. B. West, J. C. Mather, J. P. Doane, J. A. Higgins, H. Kazemi, and M. J. Rosker, “A two-dimensional millimeter wave phase scanned lens utilizing analog electromagnetic crystal (EMXT) waveguide phase shifters,” *IEEE Transactions on Antennas and Propagation*, vol. 53, no. 1, pp. 151–159, Jan. 2005.
- [19] D. Chicherin, S. Dudorov, D. Lioubtchenko, V. Ovchinnikov, S. Tretyakov, and A. Räisänen, “MEMS-based high-impedance surfaces for millimeter and submillimeter wave applications,” *Microwave and Optical Technology Letters*, vol. 48, no. 12, pp. 2570–2573, Dec. 2006.
- [20] D. Sievenpiper, “High-impedance electromagnetic surfaces,” Ph.D. Dissertation, Dept. Elect. Eng., Univ. California, Los Angeles, CA, 1999.
- [21] C. Mias and J. H. Yap, “A varactor-tunable high impedance surface with a resistive-lumped-element biasing grid,” *IEEE Transactions on Antennas and Propagation*, vol. 55, no. 7, pp. 1955–1962, July 2007.
- [22] M. N. M. Kehn, M. Nannetti, A. Cucini, S. Maci, and P.-S. Kildal, “Analysis of dispersion in dipole-FSS loaded hard rectangular waveguide,” *IEEE Transactions on Antennas and Propagation*, vol. 54, no. 8, pp. 2275–2282, Aug. 2006.

- [23] D. M. Pozar, *Microwave Engineering*, 2nd Edition, John Wiley & Sons, Inc., New York, NY, 1998.
- [24] T. Rozzi and M. Mongiardo, *Open Electromagnetic Waveguides*, IEE Electromagnetic Waves Series 43, London, UK, IEE, 1997.
- [25] R. C. Compton, L. B. Whitbourn, and R. C. McPherdan, “Strip gratings at a dielectric interface and application of Babinet’s principle,” *Applied Optics*, vol. 23, no. 18, pp. 3236–3242, Sep. 1984.